Fabrication and characterization of silicon nanocrystals by thermal oxidation of *a*-Si:H films in air

Sandeep Kohli[a)]
Department of Chemistry, Colorado State University, Fort Collins, Colorado 80523

Jeremy A. Theil
Agilent Technologies, MS 51L-GW, 5301 Stevens Creek Boulevard, Santa Clara, California 95051

Rick. D. Snyder
Agilent Technologies, MS-23, 4380 Zeigler Road, Fort Collins, Colorado 80525

Christopher D. Rithner and Peter K. Dorhout
Department of Chemistry, Colorado State University, Fort Collins, Colorado 80523

(Received 27 June 2002; accepted 23 December 2002; published 13 February 2003)

Hydrogenated amorphous silicon (*a*-Si:H) and Si–O–H heterogeneous thin films have been examined for their potential to photoluminesce. In this study, 50 nm *a*-Si:H films were deposited and oxidized to understand how film morphology affects their optical properties. Glancing angle x-ray diffraction (XRD), x-ray reflectivity, x-ray photoelectron spectroscopy, optical absorption spectroscopy in the wavelength range 250–1000 nm, and Fourier transform infrared measurements were used to complement room temperature photoluminescence (PL) studies. The results are discussed in light of the standard models for room temperature visible PL for a-SiO$_x$:H films and silicon nanocrystals. The PL peak at 1.6 eV arises from silicon nanocrystals. Modeling this band to estimate the quantum dot size indicates that the mean silicon crystallite diameter is ~5 nm, while XRD analysis gives $\sim 9 \pm 1$ nm. The discrepancy in the estimation of crystallite size by the XRD method and PL analysis is attributed to the columnar growth of the silicon nanocrystals. © *2003 American Vacuum Society.* [DOI: 10.1116/1.1547749]

I. INTRODUCTION

Thin films comprising silicon, oxygen, and hydrogen as homogeneous and heterogeneous morphologies have been studied extensively over the past few decades for their ability to emit light by radiative recombination.[1–4] They continue to be of interest for their potential application as stable silicon-based light emitting materials. If their microstructure could be appropriately tailored, it is hoped that efficient electroluminescence could be realized. Numerous studies of various forms of silicon, silicon oxide and various hydrogenated combinations thereof, have led to a plentiful spectrum of photoluminescent bands. The most heavily studied form of Si–O–H heterostructures is porous silicon of which more than 2000 articles have been published. Confinement of charge carriers in quantum-sized nanocrystallites is the most commonly used hypothesis to explain light emission from porous Si.[5–7] Although the interest in porous Si has been stimulated by its potential for application in optoelectronic devices,[7] the degradation of the photoluminescence and mechanical instability are some of the issues that render porous silicon unsuitable for these applications.[7] Porous silicon is also being investigated for its chemical and biological applications, exploiting other characteristic properties of this material including high surface area and versatility of synthesis to produce tailored porous layers.[8] Recent reports also suggest that the porous silicon might be used in bio-implants that utilize its mechanical degradation properties.[9]

Silicon nanocrystals embedded in silicon oxide are a promising candidate for a large number of optoelectronic and photonic applications[1] due to their light-emitting ability, surface stability, and compatibility with silicon-based integrated circuit technology.[4] In the past, cosputtering,[10] ion implantation,[11] chemical vapor deposition (CVD),[12] molecular beam epitaxy,[13] and laser ablation[14] have been used to fabricate such structures. Visible luminescence at room temperature has been observed for a-SiO$_x$:H thin films prepared by a dual plasma CVD reactor.[2] Room temperature photoluminescence (PL) in the visible range has also been observed in wide gap hydrogenated amorphous silicon (*a*-Si:H).[3] These studies have yielded bands from 1.5 to 2.9 eV. At this stage reader is referred to recent review articles on porous silicon[15,16] and silicon nanocrystals,[17] which provide detailed information on the structural and optical properties of these silicon nanostructures.

Silicon nanocrystals embedded in a hydrogenated amorphous silicon oxide (a-SiO$_x$:H) matrix, both of which emit visible room temperature PL, can provide a stable light emitting silicon-based material. There have been some reports related to the formation of silicon nanocrystals in a-SiO$_x$:H film annealed at 1443 K[18,19] as well formation of silicon nanocrystals formed by cw laser-treated a-SiO$_x$:H alloys.[20] Zacharias *et al.*,[21] however, had not observed any formation of silicon nanocrystals in a-SiO$_x$:H films annealed at 573–1173 K. It has been observed by some authors[22,23] that

[a)]Author to whom correspondence should be addressed; electronic mail: skohli@lamar.colostate.edu

silicon-rich SiO_2 films with O/Si<1 formed crystallite particles when annealed at 1123 K while an annealing temperature of 1323 K was required for crystallization in films with 1<O/Si<1.9. Recently workers at Electrotechnical Laboratory, Japan[24,25] and Kim *et al.*[26] had prepared the silicon nanocrystals by rapid thermal oxidation (RTO) of *a*-Si:H[24,25] and *a*-Si films[26] in oxygen atmosphere at 1073 K[24,25] and 1273 K,[26] respectively. However these studies had been largely devoted to the electrical properties and structural properties of these devices.

In this article we report the fabrication of silicon nanocrystals by thermal oxidation of plasma enhanced CVD (PECVD) *a*-Si:H films. Our goal is to understand the properties of Si–O–H heterogeneous films made by this process to see if the material and method might be a viable route to form group IV light-emitting materials. In these studies we have observed room temperature visible PL from silicon nanocrystals as well as a-SiO_x:H films. As such, we report a systematic study of the structural, optical, and chemical properties for the as-deposited and annealed *a*-Si:H films. Glancing angle x-ray diffraction (GAXRD), x-ray reflectivity (XRR), x-ray photoelectron spectroscopy (XPS), optical absorption spectroscopy, Fourier transform infrared (FTIR), and PL studies were used to investigate the structural, chemical, electrical, and optical properties of *a*-Si:H films annealed in air and probe the growth of silicon nanocrystals embedded in an a-SiO_x:H matrix.

II. EXPERIMENT

50 nm thick *a*-Si:H films were deposited on fused silica and on Si(100) substrate by PECVD.[27] The annealing furnace was heated to the desired temperature and allowed to stabilize for 1 h. The films, deposited on silicon wafers and fused silica substrates, were placed in covered fused silica beakers and then introduced into the heated furnace. Samples were annealed for 1 h at 673, 873, and 1073 K in air. After the annealing cycle, the furnace was switched off and samples were allowed to cool to room temperature in the furnace. Before each thermal cycle, the beaker was heated to 1200 K for 6 h to ensure the removal of any contaminants that could interfere with the oxidation process of the films. Although our technique was in some ways similar to the RTO process used by some authors[24–26] there were some basic differences. First of all, the oxidation was performed in a confined volume of air (closed silica beaker) with a fixed amount of oxygen (21%); hence, mass transport likely played a vital role in the oxidation process. Second, the temperature ramp rate experienced by our films was not as fast as that experienced by the sample in RTO (100 °C/s);[26] and moreover, our samples were cooled to room temperature in the furnace after the furnace was switched off. Films on silicon wafers were used for XRR, XPS, PL, and FTIR studies. Samples deposited on fused silica were used for optical absorption spectroscopy. GAXRD studies were carried out on the films deposited on silicon as well as silica substrate.

A Brüker D-8 Discover x-ray diffraction system with a Cu x-ray source, line focus optics, and a goniometer having seven axes of motion was used in the GAXRD and XRR measurements. A Göbel mirror was placed on the primary beam side and a scintillation detector on the diffracted beam side during the measurements. A Göbel mirror comprises parabollically bent multilayers with a laterally graded period to achieve monochromatic and parallel x-ray beams in the laboratory.[28,29]

Glancing angle measurements were performed with fixed low angle of incidence and a detector scan was carried out to record the diffracted x-ray intensity as a function of 2θ. In the GAXRD measurements, a low fixed angle of incidence minimized the contribution of the substrate to the diffracted pattern due to low x-ray depth of penetration. In our case, the angles of incidence were varied from 0.25° to 0.75° in increments of 0.25° and measurements were performed with soller slits with ~0.4° separation on the diffracted beam side. For an incident angle of 0.25°, the estimated depths for the 90% contribution to the diffracted beam for Si and SiO_2 films were 0.72 and 1.12 μm, respectively. The instrument alignment was checked using a SiO_2 standard.[30] The Warren–Averbach[31] method and WIN-CRYSIZE[32] software were used to estimate the crystallite size. In the Warren–Averbach method, the average crystallite size is actually an average of column lengths (averaged over all columns in one crystallite and averaged over all crystallites in the sample) while the Scherrer equation calculates a volumetric average of crystallite size; hence, the results of average crystallite size using the Warren–Averbach method differs from crystallite size evaluated from the Scherrer equation. Throughout the remainder of the article the term crystallite size will be used for average column length estimated using the Warren–Averbach method.

XRR measurements using a knife-edge collimator (KEC) were set up to have a minimum of 1500 counts over the measurement range. The KEC ensures the optimum collimation of the primary beam without the intensity reduction of a crystal monochromator. Measurements were performed over a 2θ range of 0.3°–3.0°. The multirange data were normalized and the results were simulated using Brüker REFSIM software.[33]

XPS measurements were performed using a Physical Electronics 5800 model instrument. Monochromatic $Al_{k\alpha}$ energy, 1486.6 eV, was employed as an x-ray source. The collection angle for all the measurements was 45°. An initial survey scan (pass energy 93.9 eV, step size 0.8 eV) was done to determine the elemental composition. Integrated peak area intensities under O $1s$, Si $2p$, and C $1s$ peaks were used for estimating the relative elemental composition of the films. The integrated peak area was normalized with respect to each core level atomic sensitivity factor.[34] Scans for chemical state identification of the elements were carried out with pass energy of 58.7 eV and a step size of 0.13 eV. The MULTIPAK[35] software by Physical Electronics and XPSPEAK Version 4.1 software[36] were used for peak analysis and chemical state identification as well as presentation of data. The C $1s$ peak at 284.3 eV[34,37] was used to correct for the surface charging effect before attempting the chemical state

identification. The samples were sputtered for 1 min using Ar ions, to expose the underlying surface and then scanned for elemental composition. A sputter rate of 1.6 nm/min was determined using a standard 104 nm SiO_2 film. The thickness of SiO_2 was confirmed using spectroscopic ellipsometry. Integrated peak area intensities under the O $1s$, and Si $2p$ peaks were used for estimating the gradient in oxygen concentration across the film thickness. The integrated peak area was normalized with respect to each core level atomic sensitivity factor. The background pressure during sputtering and measurement was lower than 2×10^{-6} Pa.

Optical absorption spectroscopy, in the wavelength range 330–1000 nm, was carried out using a dual-beam Cary 500 spectrophotometer (Varian Analytical Instruments). An uncoated silica substrate was placed in the path of the reference beam. FTIR transmission measurements in the spectral range 450–4000 cm^{-1} were carried out using a Thermo Nicolet MagnaIR 760 spectrophotometer equipped with DTGS detector (KBr window) and XT–KBr beam splitter. The spectral resolution for the measurements was 4 cm^{-1}. The sample compartment was purged with nitrogen. The background spectrum, including uncoated silicon substrate, was recorded and subtracted for each measurement.

PL spectra of solid films on silicon substrates were collected with a Jobin Yvon–Spex Fluorolog-3 spectrophotometer equipped with a single grating monochromator (1200 grooves/mm) in the excitation and emission paths and a photomultiplier tube emission detector.[38] Samples were illuminated with a 450 W xenon cw source at an excitation wavelength of 480 nm. Emission spectra from thin film samples on silicon substrates were collected in "front-face" mode with a spectral resolution of 0.5 nm.[38] The spectra were analyzed using the GRAMS/AI software.[39]

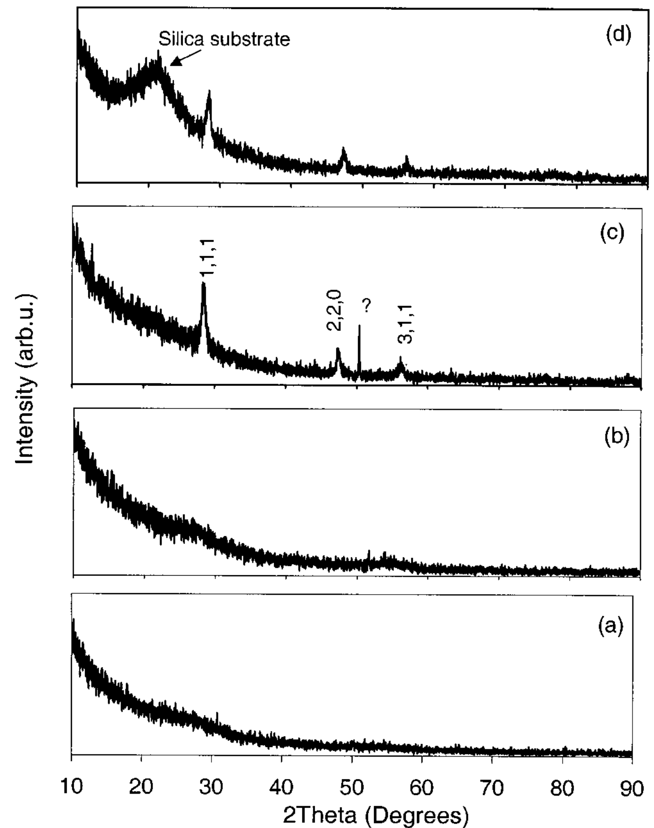

FIG. 1. GAXRD patterns for the *a*-Si:H films on the silicon substrate at a fixed angle of incidence of 0.25° annealed at: (a) 673 K, (b) 873 K, and (c) 1073 K. For comparison (d) shows the GAXRD pattern for the *a*-Si:H film on silica substrate annealed at 1073 K. The Miller indices for the silicon peaks are also shown.

III. RESULTS

A. Glancing angle x-ray diffraction

Figures 1(a)–1(c) shows the GAXRD patterns for the *a*-Si:H films deposited on silicon substrate and annealed at 673, 873, and 1073 K. GAXRD spectra are presented for measurements carried out at a fixed angle of incidence of 0.25°. The curve for the as-deposited film was similar to the film annealed at 673 K. As seen in the figure, annealing the films at 673 and 873 K did not cause any change in the diffraction pattern of the film. However, the XRD pattern for the film annealed at 1073 K showed the presence of silicon (111), (220), and (311) peaks.[40] A comparison of relative intensity with standard silicon[40] indicates the preferred orientation lies along the (111) plane. The *a*-Si:H films deposited on "silica" substrate and annealed at 1073 K also showed the presence of crystalline features and is shown in Fig. 1(d) for the sake of comparison only.

Our rationale for using two substrates is the following: the x-ray diffraction signal from silica substrate can interfere with the signal from the oxidized phase while clearly indicating the silicon crystallite formation. However for a film deposited on a silicon wafer, while the signal from silicon–oxide can be observed, the silicon peak from the silicon substrate may overlap the crystalline silicon peak from the film. The full width half maximum for XRD peaks from the silicon substrate are much narrower than for silicon nanocrystals or microcrystals. Also if the substrate were oriented it would only be coincidental that one reflection could be observed based on substrate orientation. For an ideal powder, both the 2θ–θ scan and the glancing incidence 2θ only scan will record the same diffraction pattern. However, if the sample is a single crystal (silicon wafer in our case) the two scans types will show very different data. Based on these observations, it was determined that the silicon peaks observed in Fig. 1(c) were not from the silicon substrate, but rather from the crystalline silicon phase present in the film.

Si (111) and (220) peaks [Fig. 1(c)] were chosen for the estimation of the crystallite size (Warren–Averbach method) due to the better signal-to-noise ratio. The average silicon crystallite size was found to be 9 ± 1 nm. Standard silicon powder was used for comparison and calculation of strain. Figure 2 shows the variation of relative crystallite size, cumulative crystallite size, and root-mean-square (rms) strain as a function of crystallite size. As seen in the figure, most of the crystallites had a size of 6 nm; 50% of them were smaller than 7 nm. The rms strain (arbitrary unit) values of crystallites also showed exponential dependence on crystallite size, rapidly decreasing with increasing crystallite length. Finally,

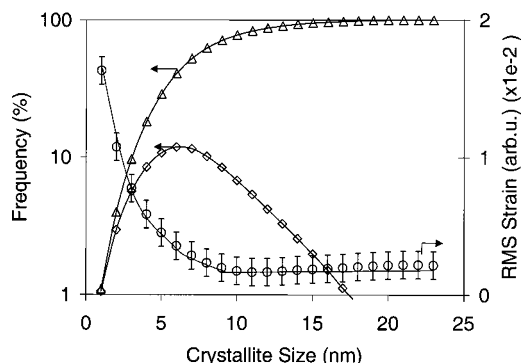

FIG. 2. (◇) Relative frequency of crystallite size, (△) cumulative frequency of crystallite size, and (○) rms strain (a. u.) as a function of crystallite size obtained using the Warren–Averbach method for XRD analysis. Standard silicon powder was used for the comparison and calculation of strain. Log scale has been used for the *Y* axis for the sake of presentation only.

the GAXRD results did not indicate the presence of crystalline SiO_2 in any of the samples.

B. X-ray reflectivity

XRR is a nondestructive technique that can be used for the estimation of thickness, density, and roughness of single-layered and multilayered thin film structures. More details for the technique are provided elsewhere.[33,41–43] The measured XRR curves for the as-deposited and annealed samples are shown in Fig. 3. The step size for the measured and simulated curves was 0.003° in theta. As seen in the figure, with increased annealing temperature, the observed Kiessig[43] fringes decayed in intensity at lower angles. This indicates that the films annealed at 873 and 1073 K had larger surface roughness as compared to the as-deposited and 673 K annealed film. The simulated XRR results are tabulated in Table I. As seen in the table, the film annealed at 673 K had higher density than the as-deposited *a*-Si:H film. However, annealing the film at 873 K did not cause any further densification of the film. The simulated results for films annealed at 1073 K indicate the presence of a low-density layer on top of the silicon film.

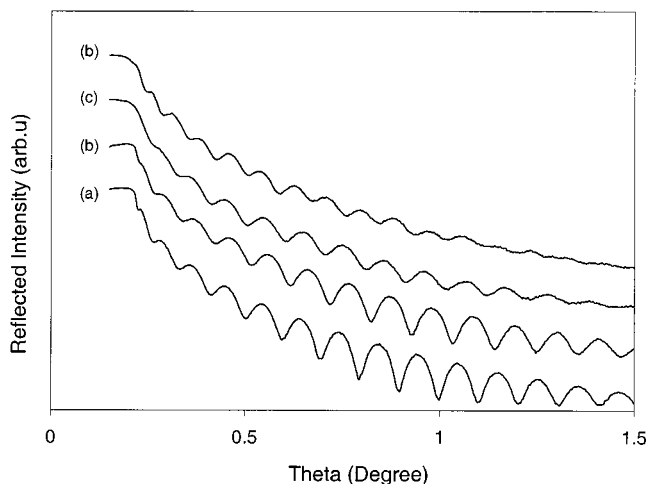

FIG. 3. Measured x-ray reflectivity curve for the: (a) as-deposited *a*-Si:H film and annealed at (b) 673 K, (c) 873 K, and (d) 1073 K. Curves are separated along the *Y* axis for the sake of presentation only.

TABLE I. Simulated XRR results for as-deposited and annealed 50 nm *a*-Si:H films.

Sample	Layer	Thickness (nm)	Density (gm/cm^3)	
As deposited	Silicon	41±1	2.12±0.05	Layer
	Silicon oxide	2±0.5	1.88±0.1	Layer
	Silicon	···	2.32	Substrate
673 K	Silicon	39±1	2.36±0.05	Layer
	Silicon oxide	2±0.5	1.94±0.1	Layer
	Silicon	···	2.32±	Substrate
873 K	Silicon	40±1	2.31±0.05	Layer
	Silicon oxide	3±1	2.09±0.1	Layer
	Silicon	···	2.32	Substrate
1073 K	Silicon oxide	2±1	1.95±0.1	Layer
	Silicon	48±1	2.29±0.05	Layer
	Silicon oxide	2±1	1.88±0.2	Layer
	Silicon	···	2.32	Substrate

C. X-ray photoelectron spectroscopy

The measured and fitted Si $2p$ XPS spectra for the as-deposited and annealed films after sputtering for 3 min are shown in Fig. 4(a). Intensity on the *Y* axis is plotted in log scale for the sake of presentation only. The Si $2p$ peaks were deconvoluted using XPSPEAK Version 4.1 software using a Gaussian–Lorentzian peak profile function and a Shirley background.[36] In the Si $2p$ spectra of the film annealed at 873 K, the peaks at ~99 eV and ~103.5 originated from Si and SiO_2, respectively. As seen in the figure, an increased annealing temperature of 1073 K led to increased formation of SiO_2 in the annealed film. The Si $2p$ line for elemental silicon is actually a doublet with the components Si $2p_{1/2}$ (Si_I^0) and Si $2p_{3/2}$ (Si_{II}^0) separated in energy by 0.6 eV and an area ratio ($A_{Si\,2p_{1/2}}/A_{Si\,2p_{3/2}}$) of 0.5.[44,45] All curves were fitted using the above constraints for the elemental silicon. After sputtering the film for 3 min, very little adventitious carbon was left on the surface that did not provide very good signal to the noise ratio for the C $1s$ peak. Although the C $1s$ peak at 284.3 eV was used to carry out a rough correction for the surface charging effect, fixing the binding energy of Si $2p_{3/2}$ to 99.5 eV provided a more accurate correction and the peak positions of all other states were shifted by the same amount. The Si $2p$ spectra can be interpreted in terms of the chemical states for Si in SiO_x: Si^0, Si^{1+}, Si^{2+}, Si^{3+}, or Si^{4+}. The binding energy for elemental silicon state is ~99.5 eV while that of fully oxidized SiO_2 (Si^{4+}) is ~103.5 eV.[34] The energy shift per Si–O bond is usually constant. Rochet *et al.*[44] had found the $Si^{4+}-Si_I^0$ energy shift to be 3.95–4.75 eV depending upon the technique used to modify the a-SiO_x thin film. The peak positions and their assigned states for our

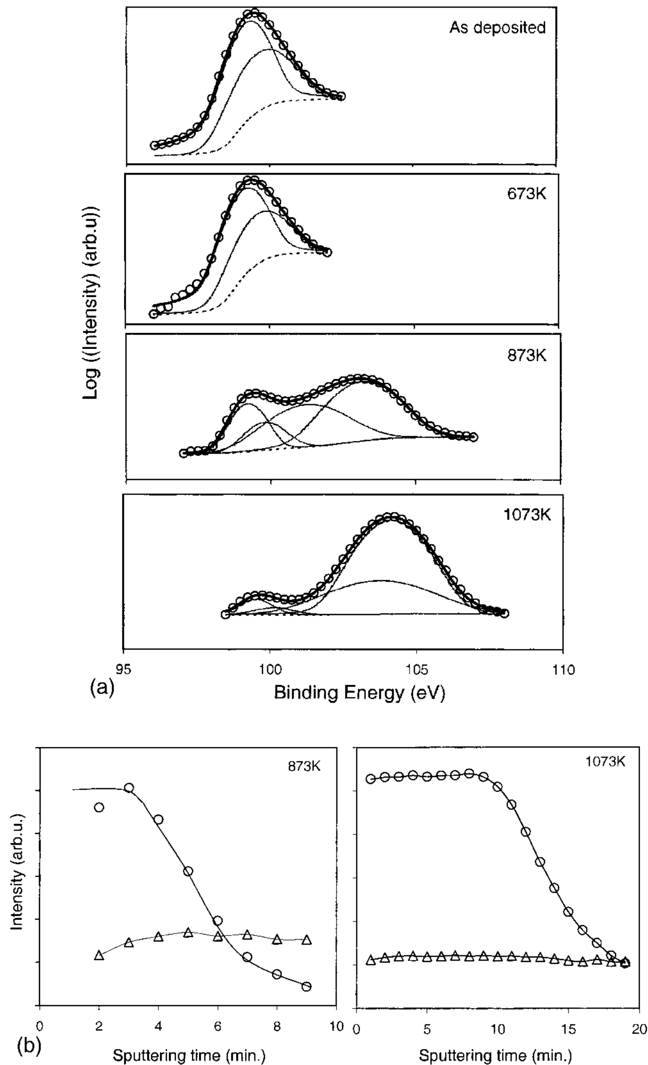

FIG. 4. (a) Measured and fitted Si $2p$ spectra for the as-deposited and annealed a-Si:H. (○) represents the measured data points, (—) represents fitted curve, (· · · ·) represents individual peaks, and (— — —) represents background. Curves have been plotted on the Y axis for the sake of presentation only. (b) Integrated peak area intensities under O $1s$ (○) and Si $2p$ (△) peaks as a function of sputtering time for a-Si:H film annealed at 873 and 1073 K.

samples are tabulated in Table II. The $Si^{4+}-Si^{0}_{I}$ energy shifts were found to be 4.3 and 4.7 eV for the samples annealed at 873 and 1073 K, respectively.

Figure 4(b) shows the integrated peak area intensities under O $1s$, and Si $2p$ peaks as a function of sputtering time. The first 1–2 min of sputtering led to the removal of adventitious carbon and oxygen, leading to the fluctuations in the integrated intensities of Si $2p$ and O $1s$ peaks. Hence these points have been ignored for the analysis. As seen in Fig. 4(b) the intensity of O $1s$ peak for film annealed at 873 K decreased to negligible values after sputtering the film for 7 min. This indicates the presence of an ~11 nm thick SiO_2 epilayer on top of the amorphous silicon film. However, for the film annealed at 1073 K, the intensity of O $1s$ peaks remained constant for about 10 min of sputtering and then gradually decreased over 9 min of additional sputtering. This indicates an increased oxidation of the film annealed at 1073 K and the presence of an oxygen gradient in the underlying buried layer. Detailed analysis of the Si $2p$ spectra, for the chemical state identification of Si, was carried out after different sputtering intervals for films annealed at 873 and 1073 K. The results have been tabulated in Tables III and IV for films annealed at 873 K and 1073 K, respectively. As seen in Tables III and IV, while the film annealed at 873 K did not have any oxide component left after being sputtered for 8 min, the film annealed at 1073 K still had some component of silicon oxide left after sputtering for 19 min. Also, the

TABLE II. Detailed peak profile analysis of Si $2p$ peak for a-Si:H films after 3 min of sputtering.

Annealing temperature	Peak position	Area	Chemical state
As deposited	99.5	66.7	Si $2p_{3/2}$
	100.1	33.3	Si $2p_{1/2}$
673 K	99.5	66.7	Si $2p_{3/2}$
	100.1	33.3	Si $2p_{1/2}$
873 K	99.5	21.0	Si $2p_{3/2}$
	100.1	10.5	Si $2p_{1/2}$
	103.1	45.8	Si^{3+}
	103.8	22.7	Si^{4+}
1073 K	99.5	3.2	Si $2p_{3/2}$
	100.1	1.6	Si $2p_{1/2}$
	104.1	27.2	Si^{4+}
	104.2	68.0	Si^{4+}

TABLE III. Detailed depth profile analysis of Si $2p$ peak for a-Si:H annealed at 873 K.

Sputtering time (min)	Peak position	Area	Chemical state
3	99.5	21.0	Si $2p_{3/2}$
	100.1	10.5	Si $2p_{1/2}$
	103.1	45.9	Si^{3+}
	103.8	22.6	Si^{4+}
4	99.5	23.2	Si $2p_{3/2}$
	100.1	11.6	Si $2p_{1/2}$
	101.6	29.6	Si^{2+}
	103.6	35.6	Si^{4+}
5	99.5	34.4	Si $2p_{3/2}$
	100.1	17.2	Si $2p_{1/2}$
	101.0	20.8	Si^{1+}
	103.3	27.6	Si^{4+}
6	99.5	46.2	Si $2p_{3/2}$
	100.1	23.1	Si $2p_{1/2}$
	101.1	17.6	Si^{1+}
	103.3	13.1	Si^{4+}
7	99.5	49.4	Si $2p_{3/2}$
	100.1	24.7	Si $2p_{1/2}$
	100.8	18.7	Si^{1+}
	103.1	07.2	Si^{3+}
8	99.5	66.7	Si $2p_{3/2}$
	100.1	33.3	Si $2p_{1/2}$

TABLE IV. Detailed depth profile analysis of Si $2p$ peak for a-Si:H annealed at 1073 K.

Sputtering time (min)	Peak position	Area	Chemical state
3	99.5	3.2	Si $2p_{3/2}$
	100.1	1.6	Si $2p_{1/2}$
	104.1	27.2	Si^{4+}
	104.2	68.0	Si^{4+}
8	99.5	2.5	Si $2p_{3/2}$
	100.1	1.3	Si $2p_{1/2}$
	103	8.6	Si^{3+}
	104.3	87.6	Si^{4+}
10	99.5	05.8	Si $2p_{3/2}$
	100.1	02.9	Si $2p_{1/2}$
	101.6	06.2	Si^{2+}
	104.2	85.1	Si^{4+}
12	99.5	17.8	Si $2p_{3/2}$
	100.1	08.9	Si $2p_{1/2}$
	101.8	13.2	Si^{2+}
	104.2	60.1	Si^{4+}
14	99.5	31.8	Si $2p_{3/2}$
	100.1	15.9	Si $2p_{1/2}$
	101.5	15.4	Si^{2+}
	104.3	36.9	Si^{4+}
16	99.5	43.8	Si $2p_{3/2}$
	100.1	21.9	Si $2p_{1/2}$
	101.5	11.9	Si^{2+}
	104.3	22.4	Si^{4+}
18	99.5	52.0	Si $2p_{3/2}$
	100.1	26.0	Si $2p_{1/2}$
	101.6	08.7	Si^{2+}
	104.4	13.1	Si^{4+}
19	99.5	56.0	Si $2p_{3/2}$
	100.1	28.0	Si $2p_{1/2}$
	102.2	07.2	Si^{2+}
	104.5	08.8	Si^{4+}

ratios of silicon oxide to silicon $[A(Si^{1+}+Si^{2+}+Si^{3+}+Si^{4+})/A(Si\,2p_{3/2}+Si\,2p_{1/2})]$ as well as the stiochiometric to nonstiochiometric silicon oxide $[A(Si^{4+})/A(Si^{1+}+Si^{2+}+Si^{3+})]$ decreased below the top solid surface of the oxidized films.

D. Infrared spectroscopy

The FTIR absorbance spectra for the as-deposited and annealed films are shown in Fig. 5. Figure 5(a) shows the IR spectrum for the as-deposited a-Si:H film. The integrated intensity of the 880 cm^{-1} band decreased with increased annealing temperature. Si–H and SiH_2 bands, around 2000 and 2100 cm^{-1}, respectively, were also observed in as-deposited film [Fig. 5(a)].[3] As a consequence of annealing at 673 K, the integrated intensity of Si–H bands decreased by a factor of 3. As seen in Figs. 5(c) and 5(d), the Si–H and SiH_2 bands were absent in the films annealed at 873 and 1073 K and a peak corresponding to Si–O(s) appeared in the vicinity of 1075 cm^{-1}. The integrated peak intensity of the Si–O(s)

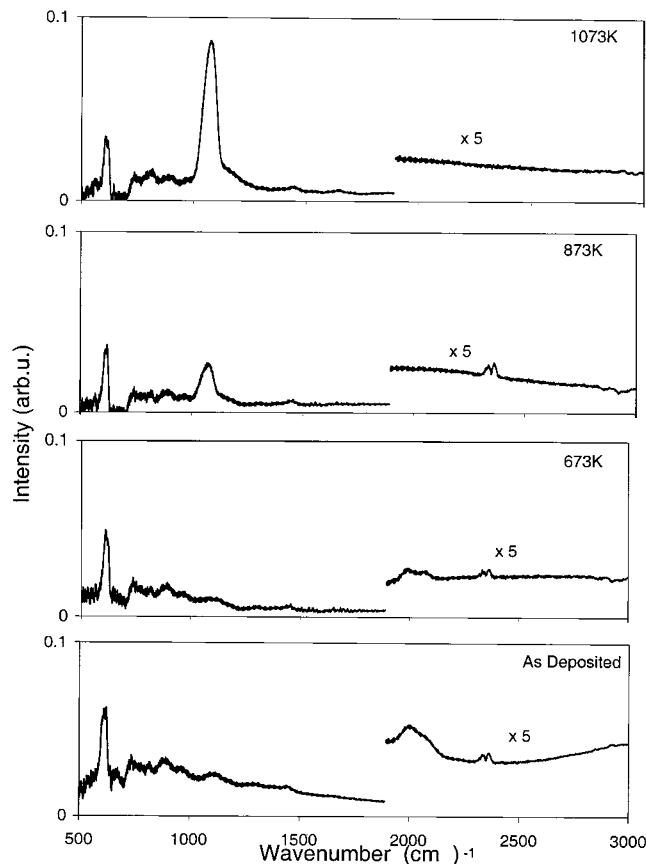

FIG. 5. FTIR absorbance spectra for the as-deposited and annealed a-Si:H films. The intensity data for points greater than 1900 cm^{-1} have been multiplied by a factor of 5 to elucidate the Si–H bands in the range 2000–2200 cm^{-1}.

vibration increased with annealing temperature. Peak analysis of the 1075 cm^{-1} band concluded that it was comprised of two peaks centered at 1075 and 1060 cm^{-1}. It has been reported that the frequency of the Si–O(s) vibration varies monotonically from 940 cm^{-1} in oxygen-doped amorphous silicon (a-SiO_x;$x=0$) to 1075 cm^{-1} in stoichiometric a-SiO_2 (a-SiO_x;$x=2$).[2,46] Using this relation we concluded that the peak at 1060 cm^{-1} corresponds to $x=1.75$ for a-SiO_x. Consequently, the films annealed at 873 and 1073 K were likely composed of stoichiometric and nonstoichiometric a-SiO_2. The band near 600 cm^{-1} was attributed to a silicon oxide layer on the substrate (Si–O terminal groups)[47] and has not been used in the analysis.

E. Optical absorption spectroscopy

Figure 6 shows the absorbance spectra in the wavelength range 330–1000 nm for as-deposited and annealed films. The optical band gaps for the films were calculated using Tauc's plot[48] defined by the relation in Eq. (1):

$$(\alpha h\nu)^{1/2}=B(h\nu-Eg), \tag{1}$$

where ν is the photon frequency in cm^{-1}, B is a constant, E_g is the Tauc's gap, and α is the optical absorption coefficient. The variation of band gap with annealing is shown in the

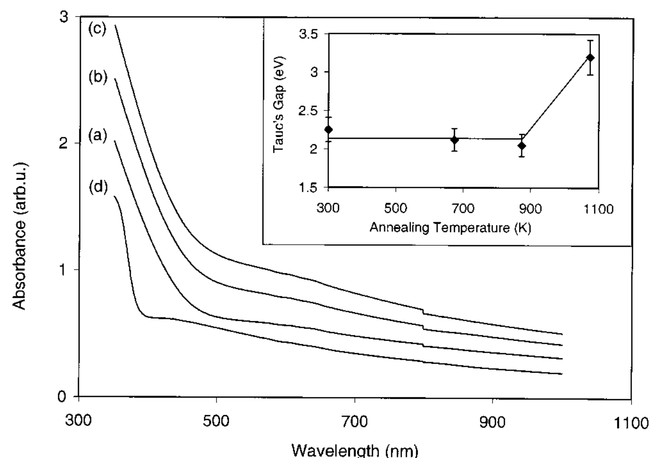

FIG. 6. Optical absorbance spectra for the as-deposited and annealed *a*-Si:H films: (a) as-deposited, (b) 673 K, (c) 873 K, and (d) 1073 K. Curves have been separated along the *Y* axis for the sake of presentation. Inset shows the variation of Tauc's band gap energy as a function of annealing temperature. 300 K has been used for the as-deposited film.

inset of Fig. 6. As seen in the curve, the band gap remained constant with the increased annealing temperature until 873 K. However, with further annealing to 1073 K, the band gap increased rapidly. We attributed this to the formation of wide-gap a-SiO_{2-x}. The optical gap of a-Si:H is around 1.7 eV and that of SiO_2 is about 10 eV.[49,50] Hence any suboxide of silicon will have an optical gap within the range of 1.7–10 eV, depending upon the composition of the alloy.[50] Singh and Davis[51] had found the Tauc's gap for a-SiO_X:H_Y to vary from 1.88 to 2.46 eV as x was changed from 0.7 to 1.5 for the a-SiO_x sample ($[H/Ar]\%=0$) and 2.0–2.9 eV for $0.7 \leqslant x \leqslant 1.5$ with $10 \leqslant [H/Ar]\% \leqslant 33$. Hamed *et al.*[52] had also found a band gap of 3.3 eV for a-SiO_X:H for $N_2O/SiH_4 = 3$. No distinct features for crystalline silicon were seen in the absorbance spectra for the film annealed at 1073 K. Finally, the volume fraction of silicon nanocrystallites seems to be large enough to appear in the XRD pattern, but low enough to be masked by a-SiO_{2-X} and/or a-SiO_X:H absorption features. This assumption was in line with GAXRD, XPS, and FTIR results for these samples.

F. Photoluminescence studies

Figure 7 shows the room temperature PL spectra for the as-deposited and annealed *a*-Si:H films. As seen in Fig. 7, the PL peak at 2.05 eV and a relatively weak/diffuse PL peak at 2.15 eV were observed for the as-deposited film. The strong peak at 2.05 eV was due to the *a*-Si:H, while the weak peak at 2.15 eV could be due to the surface-oxidized hydrogenated amorphous silicon. Room temperature PL in the range 600–1000 nm for *a*-Si:H films, with band gap in the interval 2.03–2.14 eV, had been attributed to the presence of SiH_2 and SiH_3 groups.[3] In our samples, we observed the Si–H IR band at 2085 cm^{-1}. Based on the work by Furukawa and Matsumoto,[53] we concluded that $n=1$ for $-(SiH_2)_n-(n<11)$ units in our samples.

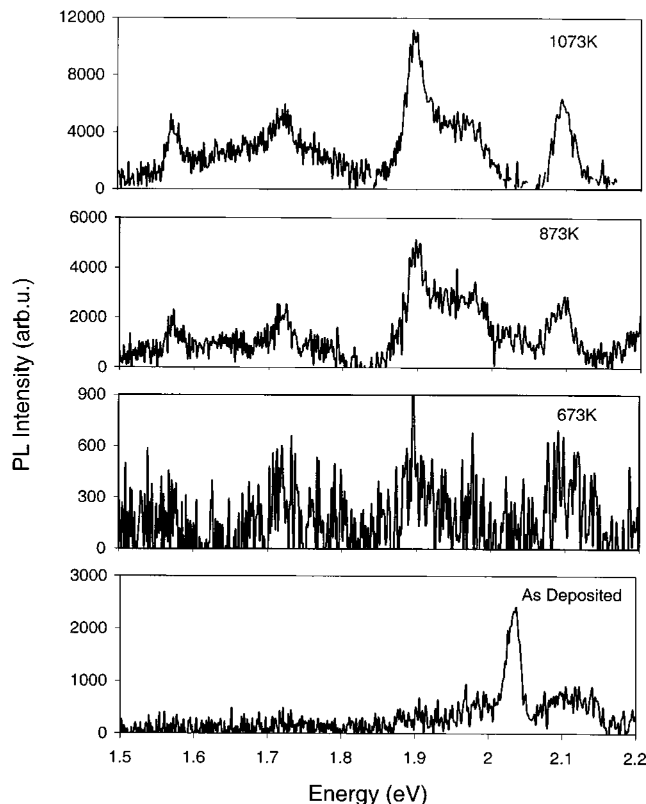

FIG. 7. Room temperature PL spectra for the as-deposited *a*-Si:H film and films annealed at 873 and 1073 K. The excitation wavelength was 480 nm and emission spectra were collected in "front-face" mode.

All of the annealed films showed very different spectra, in which the 2.05 eV band was completely absent. While the sample annealed at 673 K did not show any discernable PL bands (other than a spike in counts); PL bands appeared at 1.6, 1.7, 1.9, 2.0, and 2.1 eV for the films annealed at 873 and 1073 K. The peak at 1.7 eV was attributed to the localized-to-localized state transitions in amorphous silicon and silicon based alloys, while the peaks at 2.9 and 2.1 eV were attributed to molecular-like (or defect-like) transitions.[2] We had not observed the peak at 2.9 eV due to the excitation source (480 nm) used in the current studies. The peak at 1.9 eV was possibly due to the nonbridging oxygen-hole center ($\equiv$Si–O$^{\cdot}$).[54] The 873 and 1073 K films showed much higher levels of PL than for the as-deposited film. Finally, from 873 to 1073 K, the relative intensities of the peaks remained the same, but the overall intensity of the bands doubled in intensity.

IV. DISCUSSION

The GAXRD measurements on hydrogenated amorphous silicon films annealed at 1073 K showed the presence of 9 ± 1 nm silicon nanocrystallites, dispersed in an amorphous matrix. Differences in the coefficient of linear thermal expansion for bulk silicon (2.6×10^{-6} K^{-1}) and silicon–oxide (0.6×10^{-6} K^{-1}) caused the strain to occur in the silicon nanocrystals. However, no data are available for the variation of coefficient of thermal expansion for silicon nanocrystals

with a larger surface to volume ratio as compared to the bulk materials. The strain in the nanocrystals followed the expected inverse relation with the crystallite size, i.e., rapidly decreasing with increased crystallite size.[55–57]

The density of the as-deposited a-Si:H film estimated from the XRR measurements was lower than the crystalline silicon. This was due to its amorphous nature and the presence of hydrogen in the film. As evident from the decay of the Kiessig[43] fringes at lower angles in the XRR data, the films annealed at higher temperature exhibited higher roughness. The contributions from silicon and its oxide interfaces to the reflected intensity were weak due to the small contrast between the density of silicon and its oxide. Hence, the separation of the contributions from silicon and its oxide in the XRR curves was not only difficult to decouple but also subject to large uncertainties and error in the simulated results.

XPS results were indicative of increased oxidation of the surface as the annealing temperature was increased from 873 to 1073 K. Depth profile analysis of the film annealed at 873 K indicated the presence of about an ~11 nm epilayer of silicon oxide comprising stiochiometric and nonstiochiometric SiO_2. Oxygen content decreased rapidly below the surface of the oxide layer. However the film annealed at 1073 K, comprised approximately the top half-layer of oxide with constant oxygen concentration while the other half-layer of the oxide had an oxygen gradient decreasing toward the silicon interface. Detailed analysis of Si $2p$ spectra after 3 min of sputtering indicated that the oxide surface of the film annealed at 1073 K was completely oxidized or stiochiometric. The absence of a nonstiochiometric component of silicon oxide in the detailed analysis was due to the surface sensitive nature of XPS. The inelastic mean free path (IMFP) had been defined as the average of the distances, measured along the trajectories, that particles with a given energy travel between inelastic collisions in a substance.[34,58] The estimated values of IMFP for Si and SiO_2, at energies corresponding to Al $K\alpha$ x rays were ~3.2 and 4.0 nm, respectively.[59]

For the films annealed at 873 and 1073 K, detailed analysis of the Si $2p$ spectra after different sputtering intervals clearly indicated that the film surface toward the silicon interface had a lower oxidation state as compared to the top surface of the film. Finally, the XRD measurements did not indicate the presence of crystalline SiO_2 peaks, hence the oxidation of amorphous silicon under the present conditions led to the formation of amorphous silicon–oxide.

As seen in the IR results, annealing the film in air at 673 K led to the loss of Si–H and SiH_2 units, leading to hydrogen gas evolution. However, the loss of these units and hydrogen was not completed at 673 K, as Si–H peaks were still observed. Increasing the annealing temperature to 873 K led to the complete loss of Si–H and SiH_2 accompanied by H_2 and possibly H_2O evolution from the film. No peaks corresponding to Si–H and SiH_2 were observed within the detection limit of the instrument for the sample annealed at 873 K. The annealing at 873 K also led to limited oxidation of the film as supported by the presence of two new peaks in the vicinity of 1075 cm^{-1}, suggesting that the oxidation of the film generated stoichiometric and nonstoichiometric a-SiO_2. Increasing the annealing temperature led to an increase in area of the peaks around 1075 cm^{-1}. The integrated intensity of the peak for stoichiometric a-SiO_2 increased by a factor of 2.4 and the integrated intensity of peak for nonstiochiometric a-SiO_2 increased by a factor of 4.7 as temperature increased. Also, with the increased annealing temperature, the ratio of integrated intensity for a-SiO_{2-x}:H to a-SiO_2:H increased from 1.8 to 3.5. This behavior could be attributed to the limited volume of the air in which the sample was heated, suggesting that mass transport limited the reaction rate.

The PL data showed that the annealing processes, to which these films were subjected, resulted in crystallite formation at temperatures as low as 873 K. As heating occurred, the hydrogen within the a-Si:H evolved, leaving behind a high density of dangling bonds that acted as nonradiative recombination centers and quenched the PL signal. This was supported by the loss of the 2.05 eV band during heating. At the same time, they acted as sites for the initiation of the evolution of small crystallites. Simultaneously, oxidation of the film occurred. The oxidation may have led to an initial alloy of dehydrogenated amorphous silicon, silicon nanocrystals, and silicon oxide. The formation of the band at 1.7 eV could be caused by the remaining dehydrogenated amorphous silicon regions that were allowed to PL since they were electrically isolated from adjacent regions, thus localizing carriers. As annealing progressed, oxidized fraction of the film increased, leading to the evolution of the strong 1.9 eV band.

We attributed the peak at 1.6 eV in the PL spectra of the a-Si:H film annealed at 873 K to the growth of quantum confined silicon nanocrystals in the a-SiO_x:H matrix. Lack of silicon features in the XRD pattern for this film could be due to the low volume fraction of silicon nanocrystals in the sample, which do not effectively contribute to the diffracted intensity. However, with increased annealing temperature (1073 K) increased oxidation of the film occurred. This not only led to the formation of a more nonstoichiometric a-SiO_{2-x}:H in the film, but also led to the increased growth of silicon nanocrystals. With increased annealing, the PL peak at 1.6 eV did not shift. This indicated that the crystallite size of the silicon nanocrystals remained constant with annealing, although their volume fraction increased with annealing.

Chen *et al.*[60] modeled the contribution of quantum confinement to luminescence from silicon nanoclusters. Trwoga *et al.*[61] extended this model taking into consideration the oscillator strength as a function of an increasing crystal diameter. Quantum confinement effects are only significant for systems in which the Bohr radius of the exciton is on the order of or larger than the size of the confined system. For silicon, the bulk exciton Bohr diameter ($2a_B$) is $\simeq$10 nm. In a semiconductor, quantum confinement leads to an increase in the band gap energy and an associated increased probability of radiative transfer.[61] Based on the model for the luminescence spectrum of silicon nanocrystals by Chen *et al.* and

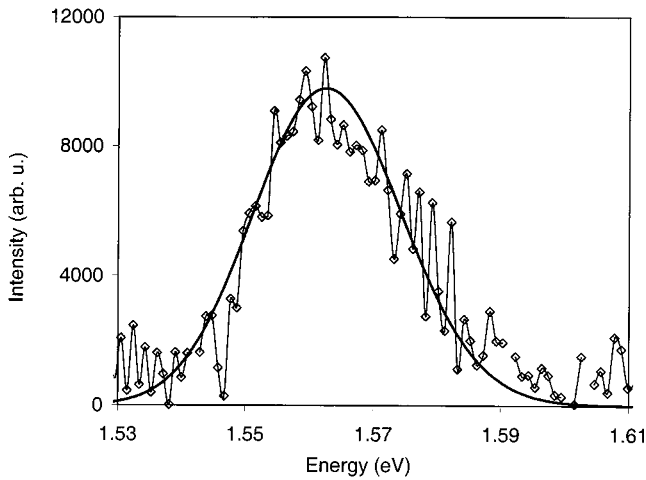

FIG. 8. Calculated (— — —) and experimental (—) PL spectra for the silicon nanocrystals on the basis of model proposed by Chen *et al.* and extended by Trwoga *et al.* The diameter of silicon nanocrystal was estimated to be 5.13 nm with a standard deviation of 1.2%.

extended by Trwoga *et al.*, assuming the radiative recombination of confined excitons to be the major contributor to the luminescence spectra, the spectrum $S(\Delta E)$ can be represented as

$$S(\Delta E)=P(\Delta E)\times f(\Delta E). \tag{2}$$

Here $P(\Delta E)$ is the line shape of the luminescence spectrum due to the quantum confinement of the silicon nanocrystals, taking into account the increase in electron–hole pairs with increasing size, and is defined as[60]

$$P(\Delta)=\frac{K}{\Delta E^3}\exp\left\{-\frac{1}{2}\left(\frac{d_0}{\sigma}\right)^2\left[\left(\frac{\Delta E_0}{\Delta E}\right)^{1/2}-1\right]^2\right\}. \tag{3}$$

Also

$$\Delta E=h\omega-(E_g-E_b), \tag{4}$$

where E_g is the bulk silicon band gap, E_b is the exciton binding energy, and

$$\Delta E_0=c/d^2, \tag{5}$$

where c is the proportionality constant (1323 eV Å^2),[60] d the crystal diameter, d_0 the mean cluster diameter, σ the standard deviation, and K the normalization constant. The expression $f(\Delta E)$ describes the oscillator strength as a function of cluster diameter and is expressed as

$$f(\Delta E)=0.15\Delta E^{2.25}. \tag{6}$$

We modeled the PL peak between 1.5 and 1.7 eV for the silicon nanocrystal on the basis of Eq. (2) with the results shown in Fig. 8. Data for this modeling were acquired for longer duration for improved signal to noise ratio. Based on the above-mentioned modeling, the estimated value of silicon nanocrystal diameter d was found to be 5.13 nm with a standard deviation of 1.2%. However, the crystallite size estimated using XRD was 9 ± 1 nm. Since the function $f(\Delta E)$ in Eq. (6) applies to the smallest dimension of an irregular crystallite,[61] this discrepancy in crystallite size can be attributed to the columnar growth of the silicon nanocrystals. It seems that the low temperature PECVD process facilitated the growth of columnar morphology for the as-deposited films. It had been shown by Tanaka *et al.*[62] that if the substrate temperature was low (<573 K), then the diffusion coefficient D_S was reduced in a-Si:H and microvoids (10–100 Å) were readily formed. Also, if films were grown with SiH_2, which has a larger sticking coefficient, hence a smaller D_S, voids and columnar structures were formed in a-Si:H, irrespective of the substrate temperature.[62,63] As the film was heated to higher temperature, hydrogen evolution from the film led to the formation of dangling bonds. The dangling bonds of Si were exposed at the surface to adsorbed and environmental oxygen present, thus causing oxidation along the voids and vacancies caused by hydrogen evolution. With increasing temperature, there was an increased oxygen diffusion into the film toward the substrate. In addition, the oxidation and oxygen diffusion appeared directional, as the oxygen only came from the top plane of the sample, leading to the columnar growth of the silicon nanocrystals.

V. CONCLUSIONS

Visible room temperature PL had been observed in the wide-gap hydrogenated amorphous silicon. The origin of this PL could be attributed to the presence of oligosilane and electron–hole recombination in tail states of hydrogenated amorphous silicon. Absence of discernable features in the room temperature PL spectra of the sample annealed at 673 K could be attributed to the loss of hydrogen and creation of dangling bonds that acted as nonradiative defect centers. With an increased annealing temperature of 873 K, PL peaks corresponding to a-SiO_{2-x}:H, nonbridging oxygen hole centers ($\equiv$Si–O$^{\cdot}$) and silicon nanocrystals appeared. However, the XRD pattern did not show the presence of crystalline silicon nanocrystals. This could be attributed to the low volume fraction of silicon nanocrystals, which did not effectively contribute to the diffracted x-ray intensity. As the samples were heated to 1073 K, weak PL peaks became more pronounced. Although the XRD pattern showed the presence of silicon nanocrystals with an average crystallite size of 9 ± 1 nm, the PL peak did not shift in energy. This indicated that annealing at 1073 K led to the isolated growth of silicon nanocrystals, thus causing the increased volume fraction of the silicon nanocrystals without the increase in the crystallite size of the nanocrystals. The luminescence spectrum for silicon nanocrystals at 1073 K was modeled and the value of the silicon crystal size was estimated to be ~5 nm. The discrepancy in the estimated crystal size on the basis of PL and XRD analysis was attributed to the columnar growth of silicon nanocrystals, since the function for the oscillator strength $f(\Delta E)$ applied to the smallest dimension of the irregular crystal. The low temperature PECVD process facilitates the growth of columnar morphology for the as-deposited films. This allowed for preferred oxidation along the void and vacancies caused by hydrogen evolution from the sample. In addition, the oxidation was directional, as the oxygen only came from the top plane of the sample, leading

to the columnar growth of the silicon nanocrystals. It should also be noted that the PL signal from our samples was weak as compared to those reported for other silicon nanostructures in the literature, some of which are cited here.[15,17,20,64] This could be a result of large defect centers/dangling bonds that were created by structural ordering, oxidation, and hydrogen removal from films. These nonradiative defect centers quench the PL signal. Annealing the films in forming gas would reduce the density of these defect centers, thereby improving the intensity of the PL signal.

ACKNOWLEDGMENTS

The authors would like to acknowledge the financial support provided by the NSF instrument Grant Nos. NSF-CHE-9808024 and NSF-DMR-0076180. Acknowledgements are also due to Dr. Pat McCurdy for help with XPS measurements.

[1] L. Brus, in *Semiconductor and Semimetals*, edited by D. Lockwood (Academic, New York, 1998), Vol. 49, p. 303.
[2] M. Zhu, Y. Han, R. B. Wehrspohn, C. Godet, R. Etemadi, and D. Ballutaud, J. Appl. Phys. **83**, 5386 (1998).
[3] J. Dian, J. Valenta, J. Hala, A. Poruba, P. Horvath, K. Luterova, I. Gregora, and I. Pelant, J. Appl. Phys. **86**, 1415 (1999).
[4] B. Garrido Fernandez, M. Lopez, C. Garcia, A. Perez-Rodriguez, J. R. Morante, C. Bonafos, M. Carrada, and A. Claverie, J. Appl. Phys. **91**, 798 (2002).
[5] L. T. Canham, Phys. Status Solidi B **190**, 9 (1994).
[6] R. T. Collins, P. M. Fauchet, and M. A. Tischler, Phys. Today **50**, 24 (1997).
[7] J. H. Song and M. J. Sailor, Inorg. Chem. **37**, 3355 (1998).
[8] M. P. Stewart and J. M. Burriak, Adv. Mater. **12**, 859 (2000).
[9] L. T. Canham, C. P. Barrett, A. P. Bowditch, T. I. Cox, and P. J. Wright, PCT Int. Appl. (1999), 75 pp. Patent No. WO 9953898A1.
[10] R. K. Soni, L. F. Fonseca, O. Resto, M. Buzaianu, and S. Z. Weisz, J. Lumin. **83–84**, 187 (1999).
[11] T. S. Iwayama, S. Nakao, and K. Saitoh, Appl. Phys. Lett. **65**, 1814 (1994).
[12] H. Takagi, H. Ogawa, Y. Yamazaki, A. Ishizadi, and T. Nakagiri, Appl. Phys. Lett. **56**, 2379 (1990).
[13] Y. Ishikawa, N. Shibata, and S. Fukatsu, Jpn. J. Appl. Phys., Part 1 **36**, 4035 (1997).
[14] T. Makimura, Y. Kunii, N. Ono, and K. Murakami, Appl. Surf. Sci. **127–129**, 388 (1998).
[15] A. G. Cullis, L. T. Canham, and P. D. Calcott, J. Appl. Phys. **82**, 909 (1997).
[16] P. M. Fauchet, J. von Behren, K. D. Hirschman, L. Tsybeskov, and S. P. Duttagupta, Phys. Status Solidi A **165**, 3 (1998).
[17] D. Kovalev, H. Heckler, G. Polisski, and F. Koch, Phys. Status Solidi B **215**, 871 (1999).
[18] Z. Ma, X. Liao, W. Zheng, J. Yu, and J. Chu, Proc. SPIE **4086**, 258 (2000).
[19] Z. Ma, X. Xiang, S. Sheng, X. Liao, C. Shao, and M. Umeno, Mater. Res. Soc. Symp. Proc. **560**, 101 (1999).
[20] M. C. Rossi, S. Salvatori, M. Burchielli, and G. Conte, Thin Solid Films **383**, 267 (2001).
[21] M. Zacharias, D. Dimova-Malinovska, and M. Stutzmann, Philos. Mag. B **73**, 799 (1996).
[22] L. A. Nesbit, Appl. Phys. Lett. **46**, 38 (1985).
[23] A. V. Dvurechenskii, F. L. Edel'man, and I. A. Ryazantsev, Thin Solid Films **91**, L55 (1982).
[24] T. Maeda, E. Suzuki, I. Sakata, M. Yamanaka, and K. Ishii, Nanobiology **10**, 127 (1999).
[25] T. Tsutsumi *et al.*, Electron. Lett. **36**, 1322 (2000).
[26] Y. Kim, K. H. Park, T. H. Chung, H. B. Bark, J.-Yel Yi, W. C. Choi, E. Y. Kim, J. W. Lee, and J. Y. Lee, Appl. Phys. Lett. **78**, 934 (2001).
[27] J. A. Theil, G. J. Kooi, and R. P. Varghese, European Patent No. 1164206 (2001), 14 pp.
[28] M. Schuster and H. Göbel, J. Phys. D **28**, A270 (1995).
[29] D. J. Nagel, J. V. Gilfrich, and T. W. Barbee, Nucl. Instrum. Methods Phys. Res. **195**, 63 (1982).
[30] JCPDS-ICDD Card No. 46-1045, International Centre for Diffraction-Data, Newton Square, PA.
[31] B. E. Warren, Prog. Met. Phys. **8**, 147 (1959).
[32] WIN-CRYSIZE Version 3.0, Crystallite Size and Microstrain, Sigma-C, München, Germany (1996).
[33] *REFSIM Version 1.2*, User's Manual (Brüker AXS GmbH, Karlsruhe, Germany, 1998).
[34] J. F. Moulder, W. F. Stickle, P. E. Sobol, and K. D. Bomben, in *Handbook of X-ray Photoelectron Spectroscopy—A Reference Book of Standard Spectra for Identification and Interpretation of XPS Data*, edited by J. Chastain and R. C. King, Jr., (Physical Electronics Inc., Eden Prairie, MN, 1995).
[35] MultiPak V6.1A, Physical Electronics Inc., Eden Prairie, MN (1999).
[36] R. M. W. Kwok, *XPSPEAK Version 4.1XPS Peak Fitting Program for WIN95/98*, http://www.phy.cuhk.edu.hk/~surface/XPSPEAK (2000).
[37] G. Johansson, J. Hedman, A. Berndtsson, M. Klasson, and R. Nilsson, J. Electron Spectrosc. Relat. Phenom. **2**, 295 (1973).
[38] *Fluorolog-3, Operation and Maintenance Manual* (Jobin Yvox-Spex Instruments S.A. Inc., Edison, NJ, 1996).
[39] *Grams/AI Version 7.0* (Thermo Galactic, Salem, NH, 1991–2001).
[40] JCPDS-ICDD Card No. 27-1402, International Centre for Diffraction-Data, Newton Square, PA.
[41] S. Kohli, C. D. Rithner, and P. K. Dorhout, J. Appl. Phys. **17**, 1149 (2002).
[42] E. Bontempi, L. E. Depero, and L. Sanagaletti, Philos. Mag. B **80**, 623 (2000).
[43] H. Kiessig, Ann. Phys. (Leipzig) **10**, 769 (1931).
[44] F. Rochet, G. Dufour, H. Roulet, B. Pelloie, J. Perriere, E. Fogarassy, A. Slaoui, and M. Forment, Phys. Rev. B **37**, 6468 (1988).
[45] A. Bansal, X. Li, S. I. Yi, W. H. Weinberg, and N. S. Lewis, J. Phys. Chem. B **105**, 10266 (2001).
[46] P. G. Pai, S. S. Chao, Y. Takagi, and G. Lucovsky, J. Vac. Sci. Technol. A **4**, 689 (1986).
[47] F. del Monte, W. Larsen, and J. D. Mackenzie, J. Am. Ceram. Soc. **83**, 628 (2000).
[48] J. Tauc, R. Grigorovici, and A. Ancu, Phys. Status Solidi **15**, 627 (1966).
[49] *Physics of Amorphous Materials*, edited by S. R. Elliot (Longman, London, 1984), p. 234.
[50] S. M. Iftiquar, J. Phys. D **31**, 1630 (1998).
[51] A. Singh and E. A. Davis, J. Non-Cryst. Solids **122**, 233 (1990).
[52] A. Hamed, H. Fritzsche, X.-M. Deng, S. Köhler, and R. Gupta, J. Non-Cryst. Solids **137–138**, 287 (1991).
[53] S. Furukawa and N. Matsumoto, Phys. Rev. B **31**, 2114 (1985).
[54] H. Nishikawa, E. Watanabe, D. Ito, Y. Sakurai, K. Nagasawa, and Y. Ohki, J. Appl. Phys. **80**, 3513 (1996).
[55] R. Delhez, Th. H. de Keijser, E. J. Mittemeijer, and J. I. Langford, Aust. J. Phys. **41**, 213 (1988).
[56] M. J. Trunen, Th. H. de Keijser, R. Dehlez, and N. M. van der Pers, J. Appl. Crystallogr. **16**, 176 (1983).
[57] D. Nesheva, Z. Levi, Z. Aneva, V. Nikolova, and H. Hofmeister, J. Phys.: Condens. Matter **12**, 751 (2000).
[58] C. J. Powell, A. Jablonski, I. S. Tilinin, S. Tanuma, and D. R. Penn, J. Electron Spectrosc. Relat. Phenom. **98–99**, 1 (1999).
[59] C. J. Powell and A. Jablonski, *NIST Electron Inelastic-Mean-Free-Path Database*-Version 1.1 (National Institute of Standards and Technology, Gaithesburg, MD, 2000).
[60] X. Chen, J. Zhao, G. Wang, and X. Shen, Phys. Lett. A **212**, 285 (1996).
[61] P. F. Trowga, A. J. Kenyon, and C. W. Pitt, J. Appl. Phys. **83**, 3789 (1998).
[62] K. Tanaka, K. Tanaka, E. Maruyama, T. Shimada, and H. Okamoto, *Amorphous Silicon*, translated by T. Sato (Wiley, New York, 1999).
[63] J. C. Knights, Jpn. J. Appl. Phys. **18**, 101 (1979).
[64] M. López, B. Garrido, C. García, P. Pellegrino, A. Pérez-Rodríguez, and J. R. Morante, J. Appl. Phys. **80**, 1637 (2002).